JACS
JOURNAL OF THE AMERICAN CHEMICAL SOCIETY
Article
pubs.acs.org/JACS

Silaindacenodithiophene-Based Molecular Donor: Morphological Features and Use in the Fabrication of Compositionally Tolerant, High-Efficiency Bulk Heterojunction Solar Cells

John A. Love,[†,§] Ikuhiro Nagao,[†,§] Ye Huang,[†] Martijn Kuik,[†] Vinay Gupta,[†,‡] Christopher J. Takacs,[†] Jessica E. Coughlin,[†] Li Qi,[†] Thomas S. van der Poll,[†] Edward J. Kramer,[†] Alan J. Heeger,[†] Thuc-Quyen Nguyen,*[,†] and Guillermo C. Bazan*[,†]

[†]Center for Polymers and Organic Solids, University of California, Santa Barbara, California 93106, United States
[‡]Organic and Hybrid Solar Cell Group, CSIR-National Physical Laboratory, New Delhi 110012, India

Supporting Information

ABSTRACT: A novel solution-processable small molecule, namely, benzo[1,2-*b*:4,5-*b*]bis(4,4′-dihexyl-4*H*-silolo[3,2-*b*]-thiophene-2,2′-diyl)bis(6-fluoro-4-(5′-hexyl-[2,2′-bithiophene]-5-yl)benzo[*c*][1,2,5]thiadiazole (p-SIDT(FBTTh$_2$)$_2$), was designed and synthesized by utilizing the silaindacenodithiophene (SIDT) framework as the central D^2 donor unit within the D^{1}AD^{2}AD^1 chromophore configuration. Relative to the widely studied 7,7′-[4,4-bis(2-ethylhexyl)-4*H*-silolo[3,2-*b*:4,5-*b*′]dithiophene-2,6-diyl]bis[6-fluoro-4-(5′-hexyl-[2,2′-bithiophene]-5-yl)benzo[*c*][1,2,5]thiadiazole] (p-DTS(FBTTh$_2$)$_2$), which contains the stronger donor fragment dithienosilole (DTS) as D^2, one finds that p-SIDT(FBTTh$_2$)$_2$ exhibits a wider band gap and can be used to fabricate bulk heterojunction solar cells with higher open circuit voltage (0.91 V). Most remarkably, thin films comprising p-SIDT(FBTTh$_2$)$_2$ can achieve exceptional levels of self-organization directly via solution deposition. For example, high-resolution transmission electron microscopy analysis shows that p-SIDT(FBTTh$_2$)$_2$ spin-cast from chlorobenzene organizes into crystalline domains with lattice planes that extend over length scales on the order of hundreds of nanometers. Such features suggest liquid crystalline properties during the evolution of the film. Moreover, grazing incidence wide-angle X-ray scattering analysis shows a strong tendency for the molecules to exist with a strong "face-on" orientation relative to the substrate plane. Similar structural features, albeit of more restricted dimensions, can be observed within p-SIDT(FBTTh$_2$)$_2$:PC$_{71}$BM bulk heterojunction thin films when the films are processed with 0.4% diiodooctane (DIO) solvent additive. DIO use also increases the solar cell power conversion efficiencies (PCEs) from 1.7% to 6.4%. Of significance from a practical device fabrication perspective is that, for p-SIDT(FBTTh$_2$)$_2$:PC$_{71}$BM blends, there is a wide range of compositions (from 20:80 to 70:30 p-SIDT(FBTTh$_2$)$_2$:PC$_{71}$BM) that provide good photovoltaic response, i.e., PCE = 4−6%, indicating a robust tendency to form the necessary continuous phases for charge carrier collection. Light intensity photocurrent measurements, charge selective diode fabrication, and internal quantum efficiency determinations were carried out to obtain insight into the mechanism of device operation. Inclusion of DIO in the casting solution results in films that exhibit much lower photocurrent dependence on voltage and a concomitant increase in fill factor. At the optimum blend ratio, devices show high charge carrier mobilities, while mismatched hole and electron mobilities in blends with high or low donor content result in reduced fill factors and device performance.

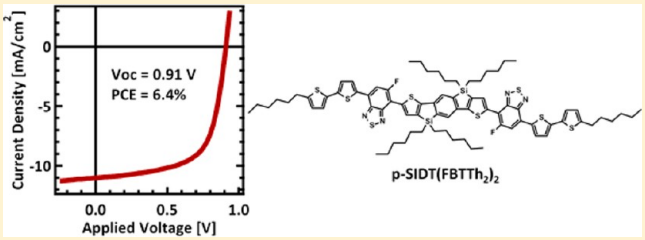

INTRODUCTION

There is increased attention on the design, fabrication, and characterization of solution-deposited bulk heterojunction (BHJ) organic solar cells in which a molecular species serves as the semiconducting donor component.[1−4] Relevant competitive aspects relative to their polymeric counterparts include the absence of a statistical distribution of molecular weights, ease of purification, and higher degree of crystallinity.[5−13] Additionally, it is possible to obtain molecular packing through single-crystal X-ray diffraction experiments.[14,15] These advantages allow a more straightforward correlation between molecular architectures and bulk properties, thereby enabling more predictive structure/property relationships.[16]

To harvest photons from a broader spectral range while maintaining large voltages, the highest achievable power conversion efficiencies (PCEs) require fabrication of tandem cells.[17−22] A primary consideration in this type of device structure is the availability of soluble semiconductors that have complementary absorption profiles and appropriate frontier orbital levels relative to each other for ensuring sufficient photocurrent generation and charge collection in the stacked,

Received: December 7, 2013
Published: February 13, 2014

 © 2014 American Chemical Society

multijunction architectures. Considering the limited examples of molecular donors with blue-shifted absorption and deep highest occupied molecular orbital (HOMO) level (arbitrarily defined here as an onset below 700 nm and deeper than −5.3 eV, respectively), which can be used to fabricate efficient devices (PCE > 6%),[12] we set our objectives toward designing such materials. Of particular interest was to consider not only molecular features, but also the organizational tendencies as a result of solution processing.

A reasonable starting point for structural design is compound p-DTS(FBTTh$_2$)$_2$ (7,7′-[4,4-bis(2-ethylhexyl)-4*H*-silolo[3,2-*b*:4,5-*b*′]dithiophene-2,6-diyl]bis[6-fluoro-4-(5′-hexyl-[2,2′-bithiophene]-5-yl)benzo[*c*][1,2,5]thiadiazole]) in Figure 1,

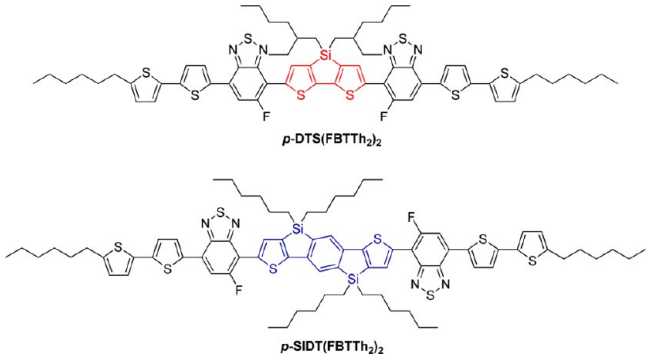

Figure 1. Molecular structures of p-DTS(FBTTh$_2$)$_2$ and p-SIDT-(FBTTh$_2$)$_2$.

which yields PCEs in excess of 8% by controlling the deposition conditions, modifying the compositions of BHJ blends with fullerene acceptors, and adjusting the device architectures.[23−25] The compound p-DTS(FBTTh$_2$)$_2$ is a part of a class of donor materials described by the D^{1}AD^{2}AD^1 molecular architecture, in which D^1 (dithiophene) and D^2 (dithienosilole, DTS) are electron-rich fragments and A (fluorobenzothiadiazole) is an electron-poor fragment.[26,27] It seemed appropriate that exchanging the internal D^2 DTS fragment with a less electron rich counterpart would result in weaker charge transfer characteristics (therefore blue-shifted absorption and a deeper HOMO level).[28] On the basis of the recent success of polymers with silaindacenodithiophene (SIDT),[29−32] we postulated that benzo[1,2-*b*:4,5-*b*]bis(4,4′-dihexyl-4*H*-silolo[3,2-*b*]thiophene-2,2′-diyl)bis(6-fluoro-4-(5′-hexyl-[2,2′-bithiophene]-5-yl)-benzo[*c*][1,2,5]thiadiazole (p-SIDT(FBTTh$_2$)$_2$) in Figure 1 would be a suitable candidate for achieving the goals set above. As a final relevant design element, p-DTS(FBTTh$_2$)$_2$ and p-SIDT(FBTTh$_2$)$_2$ keep the D^{1}A "wings" of the structure constant; only the central D^2 is different. We surmised that due to these overall structural similarities it would be possible to use previously optimized processing conditions as a starting point for exploring deposition conditions for the new material. Such considerations are worthwhile given the wide range of variables that must be investigated with a new material to optimize its function in a device.

■ RESULTS AND DISCUSSION

Synthesis and Characterization. The synthetic route to p-SIDT(FBTTh$_2$)$_2$ is provided in Scheme 1, starting with our modification for the synthesis of the SIDT unit. Rather than using the Suzuki cross-coupling method reported in the literature for the synthesis of intermediate **2**, we used a Stille

Scheme 1. Synthetic Entry into p-SIDT(FBTTh$_2$)$_2$

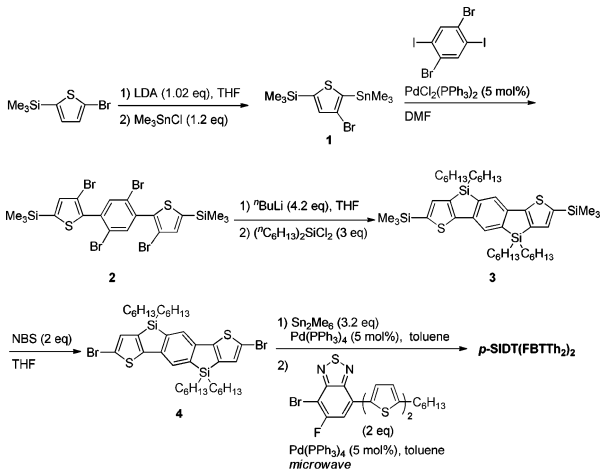

cross-coupling reaction between dibromodiiodobenzene and the stannylated thiophene **1** to obtain **2** in 70% yield. Dichlorodihexylsilane was used in the cyclization reaction with **2** to introduce the hexyl side chains in the SIDT unit and produce compound **3**. Linear hexyl side chains were utilized instead of ethylhexyl groups, as utilized by p-DTS(FBTTh$_2$)$_2$, because of our expectation that the materials would be too soluble and therefore difficult to crystallize and phase separate from fullerene in the active layer blend.[27] Reaction of **3** and *N*-bromosuccinimide gave dibrominated SIDT **4**. Palladium-catalyzed stannylation of **4** using hexamethylditin gave stannylated SIDT, which was then used in the last step of the synthetic sequence without purification in a Stille cross-coupling reaction, leading to the target p-SIDT(FBTTh$_2$)$_2$. Complete synthesis and characterization details are provided in the Supporting Information.

Figure 2a shows the optical absorption spectra of p-SIDT(FBTTh$_2$)$_2$ in solution and in the solid state. In

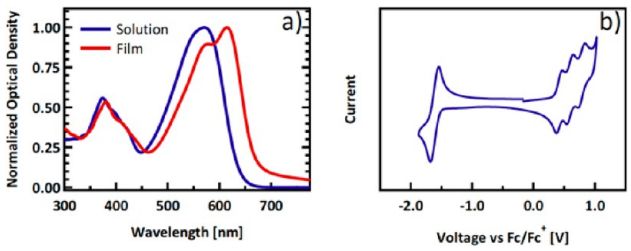

Figure 2. (a) UV−vis absorption spectra of p-SIDT(FBTTh$_2$)$_2$ in chloroform solution and in the solid state. (b) Cyclic voltammogram of p-SIDT(FBTTh$_2$)$_2$ in dichloromethane solution.

chloroform, p-SIDT(FBTTh$_2$)$_2$ shows intramolecular charge transfer absorption typical of chromophores with a D^{1}AD^{2}AD^1 architecture. One observes a low-energy transition with a maximum at 571 nm and a molar absorption coefficient of 6.5 × 10^4 M^{-1} cm^{-1}. The absorption maximum is red-shifted approximately 30 nm in thin films cast from chloroform. Additionally, there is an emergence of fine structure in the absorption profile which we attribute to molecular order in the solid state and a more planar molecular backbone structure.[33,34] From the onset of the absorption (675 nm), the solid-state optical band gap was estimated to be 1.84 eV. This is a significantly wider band gap compared to that of p-DTS-

$(FBTTh_2)_2$, whose solid-state absorption onset at 780 nm suggests a band gap of 1.50 eV. Thus, the substitution of SIDT for the central DTS unit does increase the band gap as expected. It bears noting that the solid-state absorption profile of p-SIDT$(FBTTh_2)_2$ is quite comparable to that of the archetypical donor polymer P3HT, which remains a common material employed in the wide band gap subcells of state-of-the-art tandem architectures.[20]

Cyclic voltammetry measurements of p-SIDT$(FBTTh_2)_2$ in dichloromethane were carried out to estimate the position of the frontier orbital levels, as shown in Figure 2b. From the onset of the reversible reduction and oxidation peaks, the lowest unoccupied molecular orbital (LUMO) and HOMO energy levels of p-SIDT$(FBTTh_2)_2$ were estimated as −3.36 and −5.21 eV, respectively. The electrochemical band gap of 1.85 eV is consistent with the optical band gap. Ultraviolet photoelectron spectroscopy (UPS) measurements were also used to evaluate the ionization potential of the material in the thin film and provided a value of −5.45 eV (Supporting Information). The deep HOMO level of p-SIDT$(FBTTh_2)_2$ is supported by density functional theory calculations, which predict a HOMO level of −5.4 eV (see Figure S7, Supporting Information). These complementary measurements confirm that the introduction of an SIDT unit into the molecular framework effectively pushes the HOMO level to a lower energy value relative to that of p-DTS$(FBTTh_2)_2$.[23]

While the previously noted fine structure seen in the absorption profile of p-SIDT$(FBTTh_2)_2$ suggests the presence of molecular order in the solid state, the crystalline properties of the donor material must be closely examined, as they can have a profound effect on the ability to form BHJ thin films of suitable photovoltaic performance, as observed with other small molecules.[24,35] Due to these considerations, grazing incidence wide-angle X-ray scattering (GIWAXS) was used to obtain high-resolution scattering profiles. Use of a 2-D detector allows for determination of both crystallite spacing and orientation, where χ denotes the angle from normal to the substrate.[36] Thin films of pristine p-SIDT$(FBTTh_2)_2$ were examined to probe the crystalline nature of the pure donor material. When cast from chlorobenzene, the scattering profile of p-SIDT$(FBTTh_2)_2$, shown in Figure 3, reveals strong, anisotropic texturing, as evidenced by the number of sharp, distinct peaks. Attempts to grow a single crystal of p-SIDT$(FBTTh_2)_2$ of suitable size and quality proved unsuccessful, so we cannot definitively assign peaks of the GIWAXS profile. We can, however, interpret the reflections on the basis of convention, as is commonly done with polymer systems.[36]

A strong out of plane reflection at q = 1.77 Å^{-1} is observed in Figure 3, which corresponds to a real-space distance of 3.5 Å and is attributed to intermolecular π-stacking of the conjugated backbones. This π−π distance is comparable to those of other donor molecules, including p-DTS$(FBTTh_2)_2$.[14,15,24] Note that the π-stacking peak in this film is anisotropic with respect to χ, appearing only in the out of plane direction. This indicates that p-SIDT$(FBTTh_2)_2$ must preferentially adopt a "face-on" orientation with respect to the substrate with π-stacking through the thickness of the film. The strong intensity of the peak suggests the film is relatively well ordered in the π-stacking direction, though the film is only 20−40 nm thick, which may lead to some of the broadening of the peak.[36] This orientation is in contrast to what is observed with p-DTS$(FBTTh_2)_2$, which predominantly adopts an "edge-on" orientation.[24] How such significant morphological differences arise as a function of molecular connectivity is unclear at this point, but it is worth pointing out that the face-on texture of p-SIDT$(FBTTh_2)_2$ has also been observed in a number of conjugated polymer systems containing the same SIDT donor unit.[37,38]

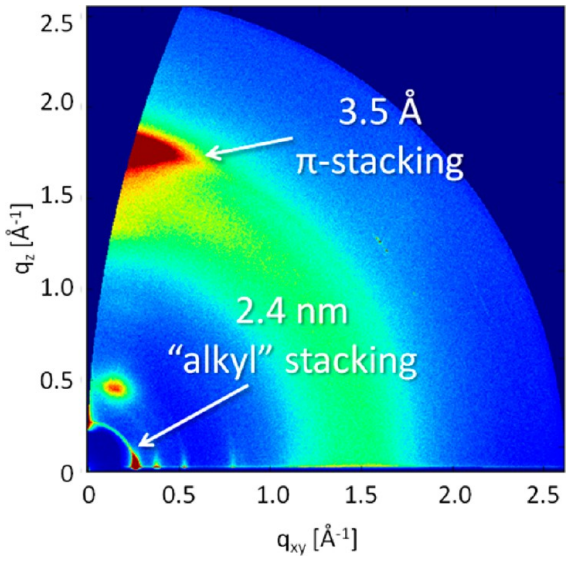

Figure 3. GIWAXS profile from a thin, pristine p-SIDT$(FBTTh_2)_2$ film.

A series of peaks at lower q values also appear in the in-plane direction. There is a sharp, intense peak at q = 0.26 Å^{-1}, which, while seen to some extent for all χ values, is considerably more evident in the in-plane direction. This corresponds to a distance of 2.4 nm in real space, which is typically associated with "alkyl stacking" or arising from columns of π-stacked units separated by alkyl side chains.[36,39,40] As π-stacking and alkyl stacking are often pseudo-orthogonal to each other, an alkyl spacing oriented in the plane of the substrate is also consistent with the proposed face-on texture.

Weaker reflections at q = 0.52 and 0.79 Å^{-1} are also observed in Figure 3 which are preferentially oriented in-plane and are assigned to the second- and third-order reflections from the alkyl stacking.[41,42] As a more quantitative measure, we can calculate the crystal correlation length (CCL), which reflects the extent of order in the crystalline lattice and increases with the crystallite size and/or perfection.[39] The Scherrer equation was used to estimate the correlation length from the peak breadths.[39,43] We find p-SIDT$(FBTTh_2)_2$ has a CCL of 37 nm. This is a relatively large CCL for molecular organic semiconductors deposited from solution and helps confirm the high degree of order in the pristine material.[36,44]

Additional features (χ = 90°, q = 0.37 Å^{-1} and at χ = 20°, q = 0.50 Å^{-1}) are also observed that are difficult to assign in the absence of a single-crystal X-ray diffraction determination. All efforts to obtain such a structure have unfortunately been unsuccessful. We therefore use the GIWAXS information to determine a strong anisotropic arrangement that strongly favors the face-on orientation.

In combination with the GIWAXS analysis, we can use transmission electron microscopy (TEM) to help understand the nature of the crystalline packing within this material. At moderately high resolution, a small level of defocus is used to shift the contrast transfer function such that phase contrast is obtained for imaging of crystal lattice planes within the film.[45−47] Avoiding electron beam damage is paramount with

this technique, as the lattice fringes can begin to disappear after only seconds. A description of the imaging process followed has been described in detail previously.[11,24] The results for TEM examination of thin films of p-SIDT(FBTTh$_2$)$_2$ are provided in Figure 4.

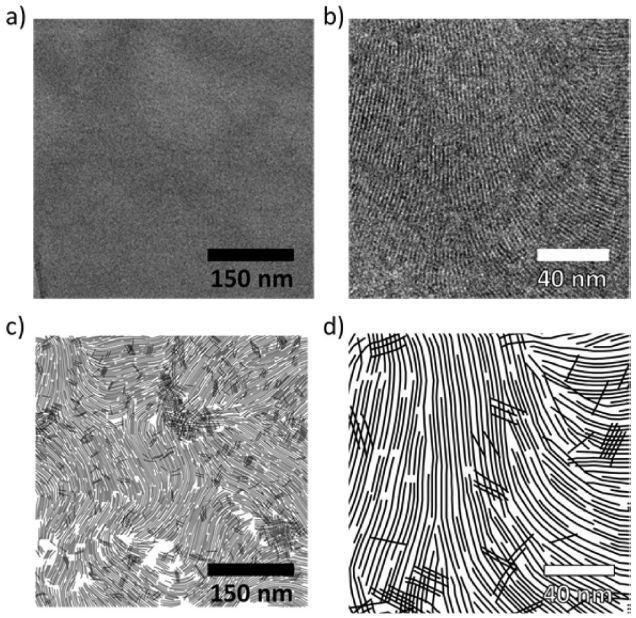

Figure 4. (a) High-resolution TEM image of a thin, pristine p-SIDT(FBTTh$_2$)$_2$ film and (b) small zoomed-in section with (c, d) corresponding flow fields showing 2.4 nm lattice spacing.

Films of pure p-SIDT(FBTTh$_2$)$_2$ show very little mass-thickness contrast on a large scale, as seen in Figure 4a. However, close examination of a blown-up section of the image (Figure 4b) reveals that crystalline lattice fringes are present across the entire image. The lattice fringes indicate a spacing of 2.4 nm, which is in good agreement with the alkyl spacing identified via GIWAXS. Due to the geometry of the electron beam, TEM is sensitive to lattices oriented in the plane of the film.[48] Thus, it is not surprising that the alkyl spacing is imaged.

The long-range ordering of the lamella across large distances (>100 nm) and the large fraction of crystalline material were surprising; the crystalline material covers nearly the entire image. As TEM is a projection through the thickness of the film, it is not possible to say if this crystalline material is predominantly located at one of the two interfaces or throughout the thickness of the film. However, the film used to obtain Figure 4 is only 20−40 nm thick, and therefore, it is reasonable to assume that the ordered regions constitute a significant volume fraction. For the sake of visual inspection, the lattice planes were identified via a simple image analysis program, and their orientation was extracted to form a director field.[49] The general directional preferences of the crystalline features identified from Figure 4a are plotted in Figure 4c. For comparison, the section of the flow field that corresponds to the portion of the image in Figure 4b is shown in Figure 4d. The director fields allow one to capture the nature of large, coherent crystalline structures that are on the order of hundreds of nanometers across. These crystalline sections bend and swirl across the film and are reminiscent of liquid crystal ordering.[50−52]

Solar Cell Fabrication and Influence of the BHJ Blend Ratio. One advantage of the SIDT unit compared to the previously used DTS unit is the presence of four alkyl groups within D^2, which promotes better solubility in common organic solvents, even with linear hexyl chains.[27] The room temperature solubility of p-DTS(FBTTh$_2$)$_2$ with ethylhexyl chains is only 5 mg/mL in chloroform, while the solubility of p-SIDT-(FBTTh$_2$)$_2$ is over 50 mg/mL in both chloroform and chlorobenzene, considerations that are relevant for processability and solar cell fabrication.

Initial solar cell performance was evaluated using the device architecture ITO/PEDOT:PSS/p-SIDT(FBTTh$_2$)$_2$:PC$_{71}$BM/Ca/Al (ITO is indium tin oxide, PEDOT:PSS is poly(3,4-(ethylenedioxy)thiophene):poly(styrenesulfonic acid), and PC$_{71}$BM is phenyl-C71-butyric acid methyl ester). A concentration of 40 mg of total solids/mL of solvent was found to give a film thickness of 100 nm and was kept constant in subsequent studies. Following the optimization of p-DTS(FBTTh$_2$)$_2$, and other structurally similar small-molecule BHJ systems,[11,23] the use of small amounts of the solvent additive diiodooctane (DIO) was first screened, and it was found that a DIO concentration of 0.4% by volume was optimum; see further discussion below.

Keeping the concentration of total solids in the solution constant at the optimum 0.4% DIO additive content, we set forth to understand the effects of systematically adjusting the p-SIDT(FBTTh$_2$)$_2$:PC$_{71}$BM blend ratio. The solar cell parameters, short circuit current (J_{SC}), open circuit voltage (V_{OC}), fill factor (FF), and PCE obtained from these studies are shown in Table 1. Optimal performance was obtained at a 50:50 weight ratio of p-SIDT(FBTTh$_2$)$_2$:PC$_{71}$BM; under these conditions, the blend can achieve J_{SC} = 11.0 mA/cm^2, V_{OC} = 0.91 V, FF = 65.0%, and PCE = 6.4%. This performance is comparable to that of some of the highest performing small-molecule systems, despite the blue-shifted absorption.[4,11−13,25]

Table 1. Photovoltaic Characteristics of Devices as a Function of the p-SIDT(FBTTh$_2$)$_2$:PC$_{71}$BM Blend Ratio

D:A	[DIO] (%, v/v)	J_{SC} (mA/cm^2)	V_{OC} (V)	FF (%)	PCE (%)
08:92	0.4	4.6	0.94	31	1.3
12:88	0.4	7.0	0.96	33	2.2
16:84	0.4	8.7	0.98	38	3.3
20:80	0.4	9.0	0.96	44	3.9
30:70	0.4	9.8	0.98	48	4.6
40:60	0.4	10.0	0.98	57	5.2
50:50	0.4	11.0	0.91	65	6.4
60:40	0.4	10.0	0.88	64	5.6
70:30	0.4	9.0	0.88	57	4.6
80:20	0.4	9.0	0.89	41	3.5
90:10	0.4	2.1	0.82	38	0.7

Closer examination of the blend ratio reveals unexpected results. Remarkably, photovoltaic efficiencies of over 3% can be maintained in blends over a range of p-SIDT(FBTTh$_2$)$_2$ content, from 80 down to 16 wt % within the blend. This stability is primarily attributed to J_{SC} values that remain relatively stable across this composition range. At 16% p-SIDT(FBTTh$_2$)$_2$, J_{SC} = 8.8 mA/cm^2, increasing to a maximum of J_{SC} = 11 mA/cm^2 for the 50:50 blend. The current then gradually decreases as the blends become more donor-rich, still achieving J_{SC} = 9.0 mA/cm^2 at 80% p-SIDT(FBTTh$_2$)$_2$.

As all films are of approximately the same thickness, on the order of 100 nm, one might expect that increasing the p-SIDT(FBTTh$_2$)$_2$ content would lead to gains in absorption and should result in larger J_{SC}. In single-pass absorption experiments (Figure 5a) high donor content does indeed lead to a significantly increased absorbance in the visible range. However, for the total device absorption in the solar cell device (Figure 5b), which includes interface scattering and reflection off the back contact,[53] the differences in total light absorbed between the blends are not particularly dramatic. Absorption of 100 nm thick films on transparent substrates shows linearly shifting absorbance profiles, but in the two-pass architecture of a solar cell with reflective contact, when viewed on a linear scale, almost regardless of composition, the film can absorb a large fraction of light. Even at only 10% donor content, the absorption in the region of 450−650 nm remains over 75%. This is due both to the good absorption of p-SIDT(FBTTh$_2$)$_2$ and to the absorption of PC$_{71}$BM in this spectral region (Figure 5b, dark blue).

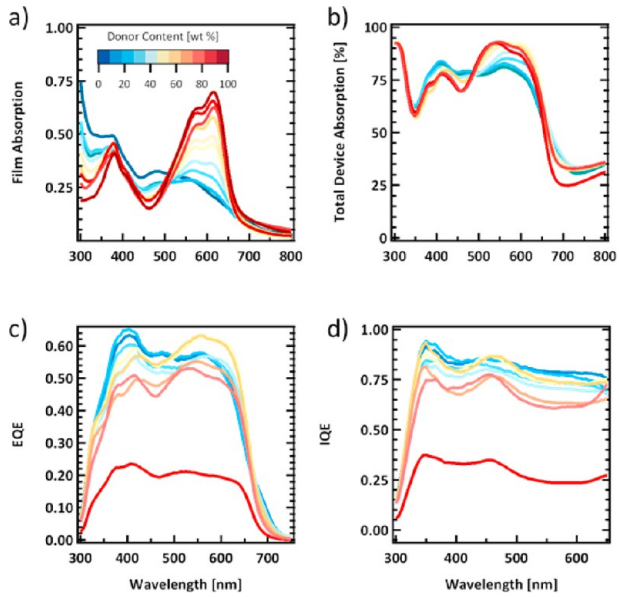

Figure 5. (a) Absorbance of p-SIDT(FBTTh$_2$)$_2$:PC$_{71}$BM films as a function of the blend ratio. (b) Total device absorption of the active layer films in a solar cell device architecture including a reflective Al back-contact. (c) External quantum efficiency and (d) internal quantum efficiency of these devices.

While good absorption is requisite for large J_{SC}, it also indicates efficient and continuous charge transport pathways from 16:84 to 80:20 blend ratios, despite the composition. Utilizing a transfer matrix model to determine the parasitic absorption from the substrate and contacts, and the measured external quantum efficiencies (EQEs; see Figure 5c) of each blend, we calculated the internal quantum efficiency (IQE) for the different ratios and provide the results in Figure 5d.[53]

Despite differences in EQE, the IQE maintains a relatively constant profile across the relevant spectral range for each blend, with only slightly higher efficiency near 400 nm due to PC$_{71}$BM absorption. IQE is highest, maintaining 80−90% efficiency across the entire spectral range, in blends with 20% p-SIDT(FBTTh$_2$)$_2$ and progressively decreases with increased donor content. The fact that the IQE in the PC$_{71}$BM absorbing region remains above 90% at such a large fullerene content indicates that nearly all of the fullerene excitons reach a p-SIDT(FBTTh$_2$)$_2$/PC$_{71}$BM interface, and despite the high acceptor content even up to 80 wt % PC$_{71}$BM, the domain size must not increase greatly past the exciton diffusion length. Furthermore, even at only 20% p-SIDT(FBTTh$_2$)$_2$, the hole transport must be sufficient to extract a large portion of the photogenerated holes at short circuit conditions to achieve such high IQE. From the IQE results, it is clear that the efficiencies of the charge generation and extraction processes are resilient toward the blend ratio. This suggests this materials system has the tendency to form a favorable morphology, with percolating phases able to effectively extract photogenerated holes and electrons, despite changes in composition.

From Table 1, in the 16:84 to 80:20 range, while J_{SC} only ranges from 8.7 to 11 mA/cm^2, the changes in FF are much greater, ranging from 38% to 65%, with the FF peaking at a 50:50 blend ratio. One explanation for the steeper dependence of the FF would be an imbalance in charge transport. Though at short circuit the charge transport may not limit extraction, a reduced hole or electron mobility may lead to a buildup of a space charge within the devices and increased bimolecular recombination at low internal fields, explaining the low FF.[54,55] Charge transport was therefore probed by fabricating single-carrier diodes using charge-selective contacts.[56] Hole-selective devices were fabricated for the different blend ratios of the solar cells, using ITO/PEDOT:PSS as the bottom contact, but incorporating a gold contact on top of the BHJ film. The work function of gold should be significantly deep enough to prevent injection of electrons into the LUMO level of the PC$_{71}$BM or p-SIDT(FBTTh$_2$)$_2$.[57,58] The electron-selective device had an Al bottom contact and Ca/Al top contact. The J−V characteristics of the devices were fit to the space charge limited current (SCLC) Mott−Gurney expression:[56]

$$J = \frac{9}{8}\varepsilon_r\varepsilon_0\mu\frac{V^2}{L^3} \tag{1}$$

where ε_0 is the vacuum permeability, ε_r is the relative dielectric constant, V is the applied voltage less the builtin voltage, L is the device thickness, and μ is the zero-field charge carrier mobility (either hole or electron). It bears noting that despite the challenge of analyzing relatively thin (100 nm) diodes, the SCLC expression fits the experimental data quite well without the need for additional parameters such as a field dependence term, see the Supporting Information. The hole and electron mobilities are plotted as a function of the blend ratio in Figure 6. At a ratio of 50:50, the hole and electron mobilities are 4×10^{-4} and 1×10^{-3} cm^2/(V s), respectively, only reduced slightly from those of the pristine materials ($\mu_{donor} = 1 \times 10^{-3}$ and $\mu_{PCBM} = 2 \times 10^{-3}$ cm^2/(V s). As the content of p-SIDT(FBTTh$_2$)$_2$ increases, and PC$_{71}$BM content is reduced, electron mobility (filled circles) is reduced. Likewise, when the cells are PC$_{71}$BM rich, the hole mobility (open squares) is reduced. When the mobility data are plotted with the solar cell parameters, as in Figure 6, it becomes clear that when either the hole or electron mobility are significantly reduced, the FF, and subsequently PCE, decreases. Thus, with a nearly constant J_{SC}, the efficiency remains high across all blend ratios in which the charge carrier mobilities are relatively balanced.

Of note is the fact that the BHJs show SCLC behavior down to 4 wt % p-SIDT(FBTTh$_2$)$_2$. This indicates that, even at such low loading, the donor phase maintains percolation such that hole transport is possible. This is below the threshold predicted on the basis of a close-packed sphere model of percolation.[59,60]

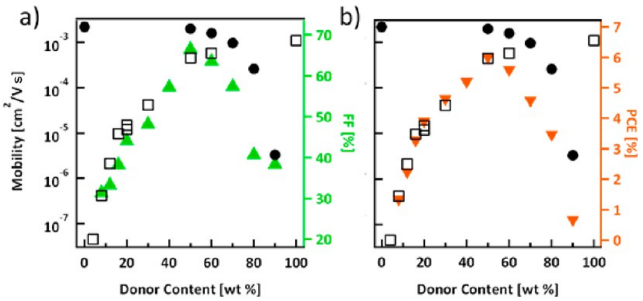

Figure 6. Electron (circles) and hole (square) mobilities across the range of p-SIDT(FBTTh$_2$)$_2$:PC$_{71}$BM blend ratios plotted showing remarkable similarities to the trends in (a) FF (green triangles) and (b) PCE (orange triangles). "Donor" on the *x*-axis refers to p-SIDT(FBTTh$_2$)$_2$.

Such a low threshold suggests the system has a tendency to assemble into an interconnected percolating nanostructure. This phase behavior would reasonably explain the ability of the active layer to maintain high J_{SC} and thus PCE across such a wide range of blend ratios.

Typically, for a percolative system in which only one phase is conductive, the conductivity, σ, can be described by the equation[59−61]

$$\sigma = \sigma_{\text{pure}}(p - p_c)^t \tag{2}$$

where p is the volume fraction of the conductive phase, p_c is the percolation threshold volume fraction, and t is the critical exponent, which has been shown to typically be equal to 2.0 for systems in three dimensions.[59,62]

If we assume that the densities of p-SIDT(FBTTh$_2$)$_2$ and PC$_{71}$BM are comparable, that is, that the weight percent of each material is approximately equal to the volume percent in the film, we can fit the mobility data to eq 3. We find empirically that the data fit best at a percolation threshold of 1.5% p-SIDT(FBTTh$_2$)$_2$ and a critical exponent of 3.0. That is

$$\mu_{\text{blend}} = \mu_{\text{pristine}}([p\text{-SIDT(FBTTh}_2)_2] - 0.015)^3 \tag{3}$$

A good fit to the experimental results indicates small perturbations in the percolation threshold have little effect on the value of t, implying that the hole mobility is indeed more sensitive to the blend ratio than should be expected from theory, which predicts t = 2.0. This may be due to the propensity for self-organization of the donor material to form domains of a particular size or shape[47] or could be caused by the presence of pure and impure phases, i.e., a mixed phase, which has also been suggested previously to result in a stronger dependence on the volume fraction.[62,63]

To fit these data well, we span nearly two decades in blend ratio and are able to fit mobilities ranging over 4 orders of magnitude from 10^{-7} to 10^{-3} cm^2/(V s) (Figure 7). We believe, even at very low donor content, the transport remains exclusively in the p-SIDT(FBTTh$_2$)$_2$ and no holes are transported through the PC$_{71}$BM phase, as pristine PC$_{71}$BM hole-only devices of the same architecture show large builtin voltages due to a large hole injection barrier from the ITO/PEDOT:PSS to its low-lying HOMO (5.8 eV).[64,65] Due to the difficulty in achieving the equivalently low leakage electron-only devices, unfortunately, we were only able to achieve a limited number of data points for electron mobilities in the blends, and a similar analysis of the percolation of PC$_{71}$BM is not possible.

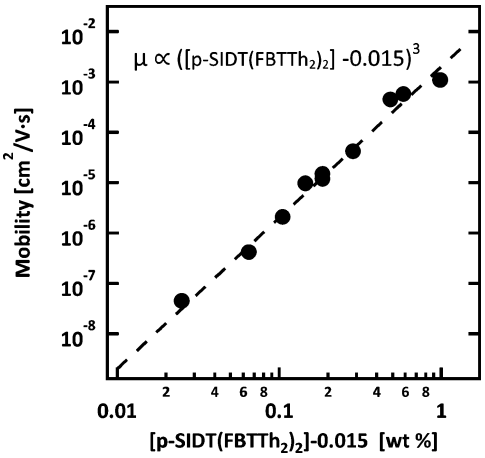

Figure 7. Hole mobility data fit to percolation eq 3 with a percolation threshold of 1.5 wt % p-SIDT(FBTTh$_2$)$_2$ and a critical exponent of 3.0.

Effects of the Solvent Additive. In the study of the blend ratio, the DIO concentration in the solvent remained fixed at 0.4% (v/v) as was found in the initial optimization of p-DTS(FBTTh$_2$)$_2$:PC$_{71}$BM solar cells. However, the full effect of addition of DIO on device performance and film morphology deserves further discussion. The complete results of this additive optimization are provided in Table 2. The V_{OC} shows a steady decrease upon addition of DIO starting from 1.0 V for devices with no additive decreasing to 0.87 V for devices processed from 1.0% DIO by volume. The increase in performance upon addition of DIO comes from the change in the FF (from 29% for no DIO to 64% with 0.4% DIO) and J_{SC} (from 5.7 mA/cm^2 for no DIO to 11.0 mA/cm^2 for 0.4% DIO). These differences cause devices prepared from pure chlorobenzene to yield PCE = 1.7%, compared to PCE = 6.4% achieved with 0.4% DIO processing. The current voltage characteristics of these devices are also shown in Figure 8. Alternatively, when the concentration of DIO in solution is increased to 1.0%, FF and J_{SC} drop to 35% and 4.1 mA/cm^2, respectively, yielding a PCE = 1.2%, thus illustrating the acute sensitivity of the active layer performance to the processing history.

Table 2. Photovoltaic Characteristics of 50:50 Devices as a Function of the DIO Concentration in the Processing Solution

[DIO] (%, v/v)	D:A	J_{SC} (mA/cm^2)	V_{OC} (V)	FF (%)	PCE (%)
0	50:50	5.7	1.00	29	1.7
0.2	50:50	7.2	0.99	34	2.5
0.4	50:50	11.0	0.91	64	6.4
0.6	50:50	9.0	0.90	62	5.0
0.8	50:50	6.1	0.87	44	2.4
1	50:50	4.1	0.87	35	1.2

Altogether, these findings are well in line with the previous optimization of p-DTS(FBTTh$_2$)$_2$ and other small-molecule systems. Without additive, the devices achieve low efficiency in large part due to low FF (29%) and J_{SC} (5.7 mA/cm^2). Each system optimizes at 0.4% DIO and shows a sharp drop off in performance when excess additive is used. This helps demonstrate that, for the SIDT for DTS substitution, the processing conditions initially determined for p-DTS-

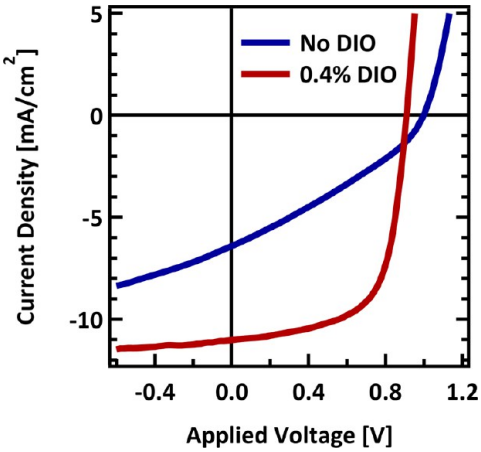

Figure 8. Current density−voltage (J−V) characteristics of 50:50 p-SIDT(FBTTh$_2$)$_2$:PC$_{71}$BM blends processed without (blue) and with (red) DIO.

(FBTTh$_2$)$_2$ provide a reasonable starting point for optimizing the structurally similar p-SIDT(FBTTh$_2$)$_2$.

In previous small-molecule BHJ systems, it has been shown that the main function of the DIO additive is to affect the nanoscale morphology.[24,66] Specifically, the increased efficiencies have been ascribed to controlling the crystallization behavior of the donor materials within the blend films, resulting in optimized domain sizes. To probe if DIO serves a similar function in this system, we carried out GIWAXS measurements on p-SIDT(FBTTh$_2$)$_2$:PC$_{71}$BM films with and without additive. There are two relatively broad peaks seen at q = 0.26 and 1.4 Å^{-1} in the scattering profile of the 50:50 p-SIDT-(FBTTh$_2$)$_2$:PC$_{71}$BM film cast from pure chlorobenzene (Figure 9a). Each is relatively diffuse and isotropic with respect to χ,

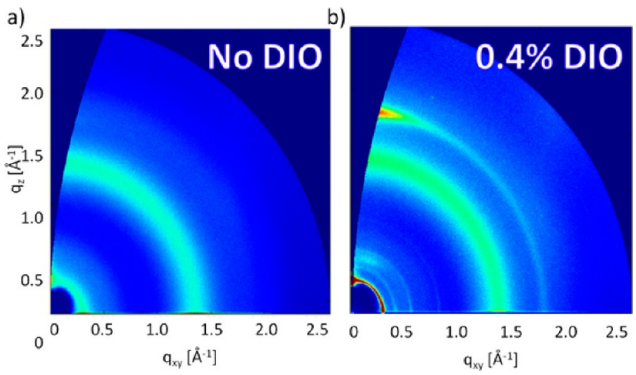

Figure 9. GIWAXS profiles of 50:50 p-SIDT(FBTTh$_2$)$_2$:PC$_{71}$BM blends processed (a) without and (b) with 0.4% (v/v) DIO.

implying random orientation within the film. The q = 1.4 Å^{-1} halo is typically attributed to amorphous scattering from the PC$_{71}$BM within the blend.[67] The peak at q = 0.26 Å^{-1} corresponds to the 2.4 nm alkyl spacing previously observed in the pristine film (Figure 3). However, the weak intensity and diffuse nature of this reflection suggest the p-SIDT(FBTTh$_2$)$_2$ is relatively disordered in the blend cast without additive.

Processing with 0.4% DIO leads to significantly more obvious scattering (Figure 9b). There is a strong π-stacking reflection at q = 1.77 Å^{-1} primarily in the out-of-plane direction. The anisotropy of the reflection with respect to χ shows that while there are some population p-SIDT(FBTTh$_2$)$_2$ crystals oriented in all directions in this film, the material preferentially π-stacks out of the plane of the substrate, as it does in the pristine film, again indicating a face-on orientation. The blend film also shows in-plane peaks at q = 0.26, 0.37, and 0.52 Å^{-1}, and though they are less intense and less anisotropic with respect to χ compared to those in the pristine film, they are consistent with a face-on texture.

From the breadth of the alkyl stacking peak oriented in-plane, we can calculate the CCL to be 28 nm in the additive processed blend. This length is significantly shorter than in the pristine film, suggesting that, despite the use of solvent additive, the PC$_{71}$BM serves to break up some of the crystallization and anisotropy of the texturing. However, the CCL and appearance of higher order diffraction suggest that the p-SIDT(FBTTh$_2$)$_2$ regains quite a bit of order within the blend, particularly when compared to films cast from pure chlorobenzene. This is consistent with the results observed in the model p-DTS-(FBTTh$_2$)$_2$ system;[24] DIO aids in the crystallization of the donor material within the BHJ.

We can further probe the crystallization and phase separation behavior of these blends using TEM. When the film is processed from pure chlorobenzene, as shown in Figure 10a,

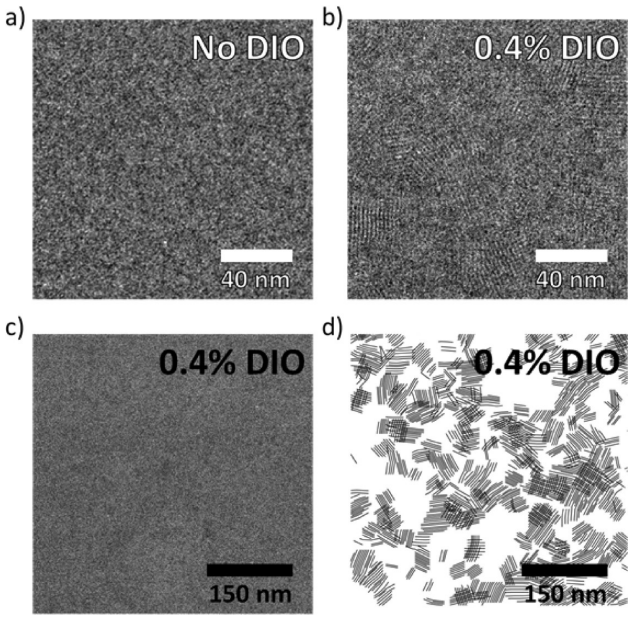

Figure 10. High-resolution TEM images of 50:50 p-SIDT-(FBTTh$_2$)$_2$:PC$_{71}$BM films, cast (a) without and (b) with 0.4% (v/v) DIO and (c) a larger area of the DIO processed film and (d) corresponding director field diagram highlighting the lattice planes.

there are no lattice fringes evident in the image. Additionally, there are no obvious larger scale features, which might arise from phase or mass-density contrast typically attributed to phase separation in the BHJ blend.[68] The relative homogeneity of the image is consistent with a molecularly well-mixed, disordered blend, consistent with the GIWAXS data.

In contrast, the p-SIDT(FBTTh$_2$)$_2$:PC$_{71}$BM film processed with 0.4% DIO shows a multitude of crystalline features throughout the area of the image, as seen by the parallel hatching in Figure 10b. The lattice spacing is at 2.4 nm, as observed with the pristine film and by GIWAXS. Though there is little mass-thickness contrast between donor and acceptor phases on the larger scale (Figure 10c), we can use image

analysis to extract the crystalline regions imaged in larger areas. The results of this analysis are shown in the director field in Figure 10d. While there does not seem to be a uniform size or shape to the imaged crystals, they are on the order of 20−40 nm, oriented isotropically throughout the imaged area, consistent with the CCL extracted from the in-plane GIWAXS profile. In a BHJ, large phases can lead to exciton decay due to the limited diffusion length.[68] Thus, it is likely not a coincidence that, in this high-performance device, the majority of the imaged crystals are on a length scale comparable to the typical exciton diffusion length. The appearance of some larger scale phases may help to explain why IQE does not reach 100%.

To examine if the lower FF in devices cast without additive is due to the buildup of space charge,[55,54] we looked at hole and electron mobilities in each blend using single-carrier diodes as described above. All devices fit the SCLC behavior described by eq 1, and the extracted mobilities are shown below in Table 3.

Table 3. Hole (μ_h) and Electron (μ_e) Mobilities Extracted from Single-Carrier Diodes for the 50:50 p-SIDT(FBTTh$_2$)$_2$:PC$_{71}$BM Blend

	μ_h (cm^2/(V s))	μ_e (cm^2/(V s))
no DIO	1×10^{-4}	1×10^{-3}
0.4% DIO	4×10^{-4}	1×10^{-3}

The hole mobilities extracted from the $J-V$ curves for blends cast without and with DIO are 1×10^{-4} and 4×10^{-4} cm^2/(V s), respectively, while the electron mobilities remain the same, 1×10^{-3} cm^2/(V s), for both devices. These electron mobilities are not significantly reduced compared to that of pristine PC$_{71}$BM, so it does not seem that electron mobility poses a significant limitation.[65]

Changes in FF are a consequence of the charge recombination present within the devices.[69,70] As an initial investigation into the recombination mechanisms, the solar cell performance was tested over a range of incident light intensities,[71−73] the results of which are shown in Figure 11. The photocurrent ($J_{photo} = J_{light} - J_{dark}$) is plotted against the effective voltage, that is, the voltage at which no photocurrent is generated less the applied voltage, $V_0 - V$, at each intensity. The effective voltage determines the strength of the electric field within the device and thus the driving force for charge extraction.[74] For this type of study, devices must have sufficiently low dark current, such that it does not constitute a significant fraction of the total device current.[75] The dark current in these devices is at least an order of magnitude lower than the device current, even under only 0.015 sun illumination (Figure S10, Supporting Information).

The photocurrent in p-SIDT(FBTTh$_2$)$_2$:PC$_{71}$BM devices processed with additive quickly saturates at a low effective voltage of about 0.1 V (Figure 11b). This indicates the charge generation and extraction processes are relatively independent of the electric field. For every intensity the behavior is the same; the photocurrent increases sharply at very low fields and plateaus starting at 0.1 V. Extracting the photocurrent values as a function of the light intensity at various effective voltages from 0.04 to 1.0 V, one observes that, even at low fields, the photocurrent always follows the light intensity, with a slope of $s = 1.0$ (Figure 11d). This suggests that, even at very low fields, charge buildup due to inefficient extraction is not a problem. This is consistent with the high mobility and FF for this device.

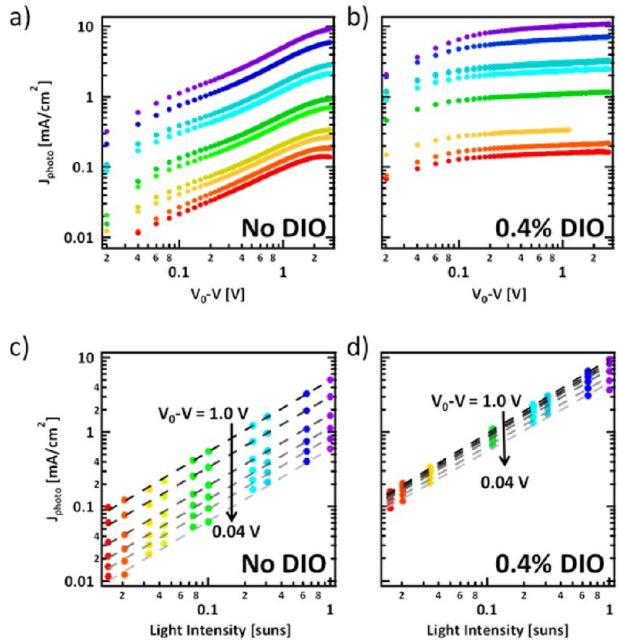

Figure 11. (a, b) Photocurrent measurements as a function of the effective voltage at various light intensities and (c, d) photocurrent measurements as a function of the light intensity at various effective voltages all fit to a slope of 1.0 for 50:50 p-SIDT(FBTTh$_2$)$_2$:PC$_{71}$BM blends processed without (a, c) and with (b, d) 0.4% (v/v) DIO.

In contrast, the photocurrent in devices cast from pure chlorobenzene does not begin to saturate even up to 3 V (Figure 11a). Instead, the photocurrent continues to increase almost linearly as a function of the electric field. This is also reminiscent of a device that is limited by charge extraction, leading to the buildup of space charge. For a device limited by insufficient extraction, the high densities of charges lead to significantly increased bimolecular recombination and thus low FF. It is expected that, in a device limited by space charge, the maximum electrostatically allowed photocurrent that can be extracted should follow a 3/4 dependence on the generation rate, which we take to be directly proportional to the light intensity, or in other words, we should expect J_{photo} to scale with the light intensity with a slope of $s = 0.75$.[54,55,76] However, from Figure 11c, it is clear that despite the extreme voltage dependence of photocurrent in the chlorobenzene cast device, this dependence does not change as a function of the internal field. Again, from 0.04 to 1.0 V of effective voltage, the device maintains a slope of $s = 1.0$. These results are not consistent with a buildup of space charge or an extraction-limited device. Together with the mobility results, these observations suggest that the strong field dependence of J_{photo} and low FF might be due to a change in charge generation with applied bias rather than simply bimolecular recombination and inefficient charge extraction.[77−80]

■ CONCLUSIONS

To summarize, a new high-efficiency molecular donor, p-SIDT(FBTTh$_2$)$_2$, with a specifically tailored energy level to improve V_{OC} has been designed and synthesized. Introduction of the "weak" SIDT donor fragment into the interior of the D^{1}AD^{2}AD^1 molecular architecture leads to blue-shifted absorption, a lower HOMO energy level, and high solubility compared with those of the previously reported DTS-containing compound. As a result of these molecular

characteristics, BHJ blends exhibit PCEs of up to 6.4% with a large V_{OC} of 0.91 V. It is worth noting that the absorption profile is well suited to integration into tandem solar cells and is comparable to that of the archetypical donor polymer P3HT, which has been demonstrated to exhibit efficiencies up to 7.4% and 6.8%, utilized in a single junction and subcell of tandem devices, respectively.[18,61] These very high efficiencies have been achieved only recently despite several years of optimization, making p-SIDT(FBTTh$_2$)$_2$ an attractive alternative.

Of particular interest for this system is the surprising nature of the blend films at different donor:acceptor ratios. For nearly all blend ratios, BHJ devices achieve IQEs above 75%, indicating that the p-SIDT(FBTTh$_2$)$_2$:PC$_{71}$BM combination can form BHJ morphologies with effective pathways for charge transport and collection across a wide range of blend compositions. We find the differences in efficiencies of the blend ratios are most strongly related to their FF, which is maximized when the charge carrier mobilities in the blend are balanced. We find that the percolation threshold for this material is remarkably low at less than 4% donor by weight, which may be attributed to the inherent nature of the material for self-assembly.

In pristine films, p-SIDT(FBTTh$_2$)$_2$ forms ordered structures on the order of hundreds of nanometers. Diffraction experiments indicate that incorporation of the SIDT unit causes the material to adopt a face-on orientation to the substrate when it crystallizes, as opposed to the edge-on orientation seen with a DTS-containing analogue. Imaging of crystalline lattice fringes via high-resolution TEM reveals liquid crystal like behavior with crystalline material spanning across nearly the entire film, while incorporation of PC$_{71}$BM to form a BHJ serves to break up this crystallization.

From a basic science perspective, it is relevant to note the similarities in the optimal BHJ composition and fabrication protocols for p-SIDT(FBTTh$_2$)$_2$ and structurally similar materials as well as in the resultant morphologies. Addition of a small amount of solvent additive is effective in inducing crystallization of the donor material in the blend, regaining some of the order seen in the pure material; the result is increased FF and J_{SC} accounting for the markedly improved performance compared with that of devices cast from pure solvent. These observations suggest that well-defined molecular donors not only provide less batch-to-batch variability than polymeric counterparts but may also enable one to more easily translate optimal processing conditions between structurally related systems.

■ ASSOCIATED CONTENT

Ⓢ Supporting Information

Synthesis and characterization of p-SIDT(FBTTh$_2$)$_2$, detailed procedures for solar cell fabrication and evaluation, and detailed procedures for morphological characterization. This material is available free of charge via the Internet at http://pubs.acs.org.

■ AUTHOR INFORMATION

Corresponding Authors

quyen@chem.ucsb.edu

bazan@chem.ucsb.edu

Author Contributions

[§]J.A.L. and I.N. contributed equally to this work.

Notes

The authors declare no competing financial interest.

■ ACKNOWLEDGMENTS

This work was supported by the Institute for Collaborative Biotechnologies through Grant W911NF-09-0001 from the U.S. Army Research Office (synthesis of new compounds) and the Center for Energy Efficient Materials, an Energy Frontier Research Center funded by the Office of Basic Energy Sciences of the U.S. Department of Energy (device evaluation and morphological characterization). The charge transport study is supported by the NSF-SOLAR program (Grant DMR-1035480). I.N. thanks the Japan Society for the Promotion of Science for a postdoctoral fellowship. V.G. acknowledges financial support from the Indo-US Science and Technology Forum (IUSSTF) (Award No. Indo-US Research Fellowship/2012-2013/26-2012). T.-Q.N. is thankful for the Camille Dreyfus Teacher Scholar Award.

■ REFERENCES

(1) Mishra, A.; Bäuerle, P. *Angew. Chem., Int. Ed.* **2012**, *51*, 2020−2067.

(2) Lin, Y.; Li, Y.; Zhan, X. *Chem. Soc. Rev.* **2012**, *41*, 4245.

(3) Walker, B.; Kim, C.; Nguyen, T.-Q. *Chem. Mater.* **2011**, *23*, 470−482.

(4) Chen, Y.; Wan, X.; Long, G. *Acc. Chem. Res.* **2013**, *46*, 2645−2655.

(5) Walker, B.; Tomayo, A. B.; Dang, X.-D.; Zalar, P.; Seo, J. H.; Garcia, A.; Tantiwiwat, M.; Nguyen, T.-Q. *Adv. Funct. Mater.* **2009**, *19*, 3063−3069.

(6) Bürckstümmer, H.; Tulyakova, E. V.; Deppisch, M.; Lenze, M. R.; Kronenberg, N. M.; Gsänger, M.; Stolte, M.; Meerholz, K.; Würthner, F. *Angew. Chem., Int. Ed.* **2011**, *123*, 11832−11836.

(7) Lee, O. P.; Yiu, A. T.; Beaujuge, P. M.; Woo, C. H.; Holcombe, T. W.; Millstone, J. E.; Douglas, J. D.; Chen, M. S.; Fréchet, J. M. J. *Adv. Mater.* **2011**, *23*, 5359−5363.

(8) Loser, S.; Bruns, C. J.; Miyauchi, H.; Ortiz, R. P.; Facchetti, A.; Stupp, S. I.; Marks, T. J. *J. Am. Chem. Soc.* **2011**, *133*, 8142−8145.

(9) Shang, H.; Fan, H.; Liu, Y.; Hu, W.; Li, Y.; Zhan, X. *Adv. Mater.* **2011**, *23*, 1554−1557.

(10) Wei, G.; Wang, S.; Sun, K.; Thompson, M. E.; Forrest, S. R. *Adv. Energy Mater.* **2011**, *1*, 184−187.

(11) Sun, Y.; Welch, G. C.; Leong, W. L.; Takacs, C. J.; Bazan, G. C.; Heeger, A. J. *Nat. Mater.* **2011**, *11*, 44−48.

(12) Zhou, J.; Zuo, Y.; Wan, X.; Long, G.; Zhang, Q.; Ni, W.; Liu, Y.; Li, Z.; He, G.; Li, C.; Kan, B.; Li, M.; Chen, Y. *J. Am. Chem. Soc.* **2013**, *135*, 8484−8487.

(13) Zhou, J.; Wan, X.; Liu, Y.; Zuo, Y.; Li, Z.; He, G.; Long, G.; Ni, W.; Li, C.; Su, X.; Chen, Y. *J. Am. Chem. Soc.* **2012**, *134*, 16345−16351.

(14) Kim, C.; Liu, J.; Lin, J.; Tamayo, A. B.; Walker, B.; Wu, G.; Nguyen, T.-Q. *Chem. Mater.* **2012**, *24*, 1699−1709.

(15) Liu, J.; Walker, B.; Tamayo, A.; Zhang, Y.; Nguyen, T.-Q. *Adv. Funct. Mater.* **2013**, *23*, 47−56.

(16) Zhugayevych, A.; Postupna, O.; Bakus, R. C., II; Welch, G. C.; Bazan, G. C.; Tretiak, S. *J. Phys. Chem. C* **2013**, *117*, 4920−4930.

(17) Hadipour, A.; de Boer, B.; Wildeman, J.; Kooistra, F. B.; Hummelen, J. C.; Turbiez, M. G. R.; Wienk, M. M.; Janssen, R. A. J.; Blom, P. W. M. *Adv. Funct. Mater.* **2006**, *16*, 1897−1903.

(18) Kim, J. Y.; Lee, K.; Coates, N. E.; Moses, D.; Nguyen, T.-Q.; Dante, M.; Heeger, A. J. *Science* **2007**, *317*, 222−225.

(19) Dennler, G.; Scharber, M. C.; Ameri, T.; Denk, P.; Forberich, K.; Waldauf, C.; Brabec, C. J. *Adv. Mater.* **2008**, *20*, 579−583.

(20) You, J.; Dou, L.; Yoshimura, K.; Kato, T.; Ohya, K.; Moriarty, T.; Emery, K.; Chen, C.-C.; Gao, J.; Li, G.; Yang, Y. *Nat. Commun.* **2013**, *4*, 1446.

(21) Dou, L.; You, J.; Yang, J.; Chen, C.-C.; He, Y.; Murase, S.; Moriarty, T.; Emery, K.; Li, G.; Yang, Y. *Nat. Photonics* **2012**, *6*, 180−185.

(22) Li, W.; Furlan, A.; Hendriks, K. H.; Wienk, M. M.; Janssen, R. A. J. *J. Am. Chem. Soc.* **2013**, *135*, 5529−5532.
(23) Van der Poll, T. S.; Love, J. A.; Nguyen, T.-Q.; Bazan, G. C. *Adv. Mater.* **2012**, *24*, 3646−3649.
(24) Love, J. A.; Proctor, C. M.; Liu, J.; Takacs, C. J.; Sharenko, A.; van der Poll, T. S.; Heeger, A. J.; Bazan, G. C.; Nguyen, T.-Q. *Adv. Funct. Mater.* **2013**, *23*, 5019−5026.
(25) Gupta, V.; Kyaw, A. K. K.; Wang, D. H.; Chand, S.; Bazan, G. C.; Heeger, A. J. *Sci. Rep.* **2013**, *3*, 1−6.
(26) Welch, G. C.; Perez, L. A.; Hoven, C. V.; Zhang, Y.; Dang, X.-D.; Sharenko, A.; Toney, M. F.; Kramer, E. J.; Nguyen, T.-Q.; Bazan, G. C. *J. Mater. Chem.* **2011**, *21*, 12700−12709.
(27) Henson, Z. B.; Welch, G. C.; van der Poll, T.; Bazan, G. C. *J. Am. Chem. Soc.* **2012**, *134*, 3766−3779.
(28) Duan, C.; Huang, F.; Cao, Y. *J. Mater. Chem.* **2012**, *22*, 10416.
(29) Ashraf, R. S.; Schroeder, B. C.; Bronstein, H. A.; Huang, Z.; Thomas, S.; Kline, R. J.; Brabec, C. J.; Rannou, P.; Anthopoulos, T. D.; Durrant, J. R.; McCulloch, I. *Adv. Mater.* **2013**, *25*, 2029−2034.
(30) Ashraf, R. S.; Chen, Z.; Leem, D. S.; Bronstein, H.; Zhang, W.; Schroeder, B.; Geerts, Y.; Smith, J.; Watkins, S.; Anthopoulos, T. D.; Sirringhaus, H.; de Mello, J. C.; Heeney, M.; McCulloch, I. *Chem. Mater.* **2011**, *23*, 768−770.
(31) Schroeder, B. C.; Huang, Z.; Ashraf, R. S.; Smith, J.; D'Angelo, P.; Watkins, S. E.; Anthopoulos, T. D.; Durrant, J. R.; McCulloch, I. *Adv. Funct. Mater.* **2012**, *22*, 1663−1670.
(32) Wang, J.-Y.; Hau, S. K.; Yip, H.-L.; Davies, J. A.; Chen, K.-S.; Zhang, Y.; Sun, Y.; Jen, A. K.-Y. *Chem. Mater.* **2011**, *23*, 765−767.
(33) Mizuguchi, J. *J. Phys. Chem. A* **2000**, *104*, 1817−1821.
(34) Erb, T.; Zhokhavets, U.; Gobsch, G.; Raleva, S.; Stühn, B.; Schilinsky, P.; Waldauf, C.; Brabec, C. J. *Adv. Funct. Mater.* **2005**, *15*, 1193−1196.
(35) Welch, G. C.; Bakus, R. C.; Teat, S. J.; Bazan, G. C. *J. Am. Chem. Soc.* **2013**, *135*, 2298−2305.
(36) Baker, J. L.; Jimison, L. H.; Mannsfeld, S.; Volkman, S.; Yin, S.; Subramanian, V.; Salleo, A.; Alivisatos, A. P.; Toney, M. F. *Langmuir* **2010**, *26*, 9146−9151.
(37) Zhang, W.; Smith, J.; Watkins, S. E.; Gysel, R.; McGehee, M.; Salleo, A.; Kirkpatrick, J.; Ashraf, S.; Anthopoulos, T.; Heeney, M.; McCulloch, I. *J. Am. Chem. Soc.* **2010**, *132*, 11437−11439.
(38) McCulloch, I.; Ashraf, R. S.; Biniek, L.; Bronstein, H.; Combe, C.; Donaghey, J. E.; James, D. I.; Nielsen, C. B.; Schroeder, B. C.; Zhang, W. *Acc. Chem. Res.* **2012**, *45*, 714−722.
(39) Rogers, J. T.; Schmidt, K.; Toney, M. F.; Kramer, E. J.; Bazan, G. C. *Adv. Mater.* **2011**, *23*, 2284−2288.
(40) Du, C.; Li, W.; Duan, Y.; Li, C.; Dong, H.; Zhu, J.; Hu, W.; Bo, Z. *Polym. Chem.* **2013**, *4*, 2773−2782.
(41) Dürr, A. C.; Schreiber, F.; Münch, M.; Karl, N.; Krause, B.; Kruppa, V.; Dosch, H. *App. Phys. Lett.* **2002**, *81*, 2276−2278.
(42) Sun, Y. M.; Ma, Y. Q.; Liu, Y. Q.; Lin, Y. Y.; Wang, Z. Y.; Wang, Y.; Di, C. A.; Xiao, K.; Chen, X. M.; Qiu, W. F.; Zhang, B.; Yu, G.; Hu, W. P.; Zhu, D. B. *Adv. Funct. Mater.* **2006**, *16*, 426−432.
(43) Langford, J. I.; Wilson, A. J. C. *J. Appl. Crystallogr.* **1978**, *11*, 102−113.
(44) Chen, D.; Nakahara, A.; Wei, D.; Nordlund, D.; Russell, T. P. *Nano Lett.* **2011**, *11*, 561−567.
(45) Lovinger, A. J.; Katz, H. E.; Dodabalapur, A. *Chem. Mater.* **1998**, *10*, 3275−3277.
(46) Martin, D. C.; Chen, J.; Yang, J.; Drummy, L. F.; Kübel, C. *J. Polym. Sci., Part B: Polym. Phys.* **2005**, *43*, 1749−1778.
(47) Kübel, C.; González-Ronda, L.; Drummy, L. F.; Martin, D. C. *J. Phys. Org. Chem.* **2000**, *13*, 816−829.
(48) Williams, D. B.; Carter, C. B. *Transmission Electron Microscopy*, 2nd ed.; Springer: New York, 2009.
(49) Takacs, C. J.; Treat, N. D.; Krämer, S.; Chen, Z.; Facchetti, A.; Chabinyc, M. L.; Heeger, A. J. *Nano Lett.* **2013**, *13*, 2522−2527.
(50) Frank, F. C. *Discuss. Faraday Soc.* **1958**, *25*, 19−28.
(51) Hu, Z.; Chen, S.; Zhang, S.; Qian, R. *Macromol. Rapid Commun.* **2000**, *21*, 1028−1031.
(52) McCulloch, I.; Heeney, M.; Bailey, C.; Genevicius, K.; MacDonald, I.; Shkunov, M.; Sparrowe, D.; Tierney, S.; Wagner, R.; Zhang, W.; Chabinyc, M. L.; Kline, R. J.; McGehee, M. D.; Toney, M. F. *Nat. Mater.* **2006**, *5*, 328−333.
(53) Burkhard, G. F.; Hoke, E. T.; McGehee, M. D. *Adv. Mater.* **2010**, *22*, 3293−3297.
(54) Mihailetchi, V. D.; Wildeman, J.; Blom, P. W. M. *Phys. Rev. Lett.* **2005**, *94*, 126602.
(55) Di Nuzzo, D.; van Reenen, S.; Janssen, R. A. J.; Kemerink, M.; Meskers, S. C. J. *Phys. Rev. B* **2013**, *87*, 085207.
(56) Coropceanu, V.; Cornil, J.; da Silva Filho, D. A.; Olivier, Y.; Silbey, R.; Brédas, J.-L. *Chem. Rev.* **2007**, *107*, 926−952.
(57) Ueno, N. In *Semiconducting Polymer Composites: Principles, Morphologies, Properties and Applications*; Yang, X., Ed.; John Wiley & Sons: Weinheim, Germany, 2012.
(58) Scheinert, S.; Grobosch, M.; Sprogies, J.; Hörselmann, I.; Knupfer, M.; Paasch, G. *J. Appl. Phys.* **2013**, *113*, 174504.
(59) Stauffer, D.; Aharony, A. *Introduction to Percolation Theory*; CRC Press: London, 1994.
(60) Sahini, M.; Sahimi, M. *Applications of Percolation Theory*; CRC Press: London, 1994.
(61) Zallen, R. *The Physics of Amorphous Solids*; John Wiley & Sons: New York, 1998.
(62) Levon, K.; Margolina, A.; Patashinsky, A. Z. *Macromolecules* **1993**, *26*, 4061−4063.
(63) Li, J.; Ray, B.; Alam, M. A.; Östling, M. *Phys. Rev. E* **2012**, *85*, 021109.
(64) Brabec, C. J.; Sariciftci, N. S.; Hummelen, J. C. *Adv. Funct. Mater.* **2001**, *11*, 15−26.
(65) Mihailetchi, V. D.; van Duren, J. K. J.; Blom, P. W. M.; Hummelen, J. C.; Janssen, R. A. J.; Kroon, J. M.; Rispens, M. T.; Verhees, W. J. H.; Wienk, M. M. *Adv. Funct. Mater.* **2003**, *13*, 43−46.
(66) Takacs, C. J.; Sun, Y.; Welch, G. C.; Perez, L. A.; Liu, X.; Wen, W.; Bazan, G. C.; Heeger, A. J. *J. Am. Chem. Soc.* **2012**, *134*, 16597−16606.
(67) Gomez, E. D.; Barteau, K. P.; Wang, H.; Toney, M. F.; Loo, Y.-L. *Chem. Commun.* **2010**, *47*, 436−438.
(68) Gunes, S.; Neugebauer, N.; Sariciftci, N. S. *Chem. Rev.* **2007**, *107*, 1324−1338.
(69) Pivrikas, A.; Sariciftci, N. S.; Juška, G.; Österbacka, R. *Prog. Photovoltaics* **2007**, *15*, 677−696.
(70) Proctor, C. M.; Kuik, M.; Nguyen, T.-Q. *Prog. Polym. Sci.* **2013**, *38*, 1941−1960.
(71) Cowan, S. R.; Roy, A.; Heeger, A. J. *Phys. Rev. B* **2010**, *82*, 245207.
(72) Koster, L. J. A.; Mihailetchi, V. D.; Ramaker, R.; Blom, P. W. M. *Appl. Phys. Lett.* **2005**, *86*, 123509.
(73) Maurano, A.; Hamilton, R.; Shuttle, C. G.; Ballantyne, A. M.; Nelson, J.; O'Regan, B.; Zhang, W.; McCulloch, I.; Azimi, H.; Morana, M.; Brabec, C. J.; Durrant, J. R. *Adv. Mater.* **2010**, *22*, 4987−4992.
(74) Mihailetchi, V. D.; Koster, L. J. A.; Hummelen, J. C.; Blom, P. W. M. *Phys. Rev. Lett.* **2004**, *93*, 216601.
(75) Dibb, G. F. A.; Kirchartz, T.; Credgington, D.; Durrant, J. R.; Nelson, J. *J. Phys. Chem. Lett.* **2011**, *2*, 2407−2411.
(76) Goodman, A. M.; Rose, A. *J. Appl. Phys.* **1971**, *42*, 2823−2830.
(77) Andersson, L. M.; Müller, C.; Badada, B. H.; Zhang, F.; Würfel, U.; Inganäs, O. *J. Appl. Phys.* **2011**, *110*, 024509.
(78) Albrecht, S.; Janietz, S.; Schindler, W.; Frisch, J.; Kurpiers, J.; Kniepert, J.; Inal, S.; Pingel, P.; Fostiropoulos, K.; Koch, N.; Neher, D. *J. Am. Chem. Soc.* **2012**, *134*, 14932−14944.
(79) Tvingstedt, K.; Vandewal, K.; Zhang, F.; Inganäs, O. *J. Phys. Chem. C* **2010**, *114*, 21824−21832.
(80) Credgington, D.; Jamieson, F. C.; Walker, B.; Nguyen, T.-Q.; Durrant, J. R. *Adv. Mater.* **2012**, *24*, 2135−2141.